Engineering of an epoxide hydrolase for efficient bioresolution of bulky pharmaco substrates

Xu-Dong Kong[a,b], Shuguang Yuan[b], Lin Li[c], She Chen[c], Jian-He Xu[a,1], and Jiahai Zhou[b,1]

[a]State Key Laboratory of Bioreactor Engineering, East China University of Science and Technology, Shanghai 200237, China; [b]State Key Laboratory of Bio-organic and Natural Products Chemistry, Shanghai Institute of Organic Chemistry, Chinese Academy of Sciences, Shanghai 200032, China; and [c]National Institute of Biological Sciences, Beijing 102206, China

Edited by James A. Wells, University of California, San Francisco, CA, and approved September 30, 2014 (received for review March 17, 2014)

Optically pure epoxides are essential chiral precursors for the production of (*S*)-propranolol, (*S*)-alprenolol, and other β-adrenergic receptor blocking drugs. Although the enzymatic production of these bulky epoxides has proven difficult, here we report a method to effectively improve the activity of *Bm*EH, an epoxide hydrolase from *Bacillus megaterium* ECU1001 toward α-naphthyl glycidyl ether, the precursor of (*S*)-propranolol, by eliminating the steric hindrance near the potential product-release site. Using X-ray crystallography, mass spectrum, and molecular dynamics calculations, we have identified an active tunnel for substrate access and product release of this enzyme. The crystal structures revealed that there is an independent product-release site in *Bm*EH that was not included in other reported epoxide hydrolase structures. By alanine scanning, two mutants, F128A and M145A, targeted to expand the potential product-release site displayed 42 and 25 times higher activities toward α-naphthyl glycidyl ether than the wild-type enzyme, respectively. These results show great promise for structure-based rational design in improving the catalytic efficiency of industrial enzymes for bulky substrates.

epoxide hydrolase | X-ray crystallography | protein engineering | product release | bulky substrate

O ca re e de a d e c re d g c a d are a ab e c ra b d g b f e c ar ace ca ac ec d a d erf e c e ca (1). E g a c e f re ar g e a re e de a d d c de e a e r c e da d dr a ef b ra e a d e re race c e de . T e e reac ca be acc ed e er c e ca ca a c a c ra a e c a c e e a d r a ga e e add c b a a c a ge a e a d e de dr a e (EH) (2–4). I e a decade , EH a e rece ed c a e beca e e are c ac - de e de e e a are "ea e" f ca a g e dr race c e de e d g e a re e de a d c a d (1, 5, 6). H e er, a ca EH ab a a d d r a e dered b e r arr b ra e c e, e a e ec , a d reg e ec , r c b (7, 8).

Ma r -e g eer g eff a e bee ade er- c e e e dra bac (9, 10). F e a e, d rec ed e b err - r e PCR DNA ff g a bee ed a ce e ac a d e a e ec EH (11–13). S r c re- g ded age e a ge era ed a fe EH ar a - r ed ca a c erf a ce (14–16). T e ra eg era e C b a a Ac e S e-Sa ra Te (CAST) c b e e ra a a r c a d d rec ed e e d g - a a d a f ed a brar e f cree g EH be er e a e ec (7, 17). B a g re d e a e b ra e- b d g e, e b ra e EH a e bee e a ded - c de c c c *meso*-e de , e g c d e er (PGE) der a- e , a d er re e de- e a a (18, 19). H e er, e ca a c eff c e c EH a fac f b e de b ra e c d g rec r (*S*)- r ra , (*S*)-a re , a d er β-adre erg c rece b g dr g (20, 21).

I , e e ec *Bm*EH, a EH c ed fr *Bacillus megaterium* ECU1001, e a d b ra e c e f b ar ac b ra e α- a g c d e er (NGE). T e - e a e a d ra b a a beca e a , a (*R*)-e a e ec a d re e *ortho*- b ed PGE a d *para*- r re e de e ce e e a er c ra (*E* > 200) (22). We f r de f ed e ac e, e *Bm*EH b g cr a r c, re c e ed a b ra e a a e - ace a de (POA) a d a a g e r e b ra e e r a d r c re ea e b a ec r a a . A a e ca g e er e arge ed e e a r c-re ea e e *Bm*EH re ed ar a , F128A a d M145A, eff c e b e ab e NGE. F r er e c ea, re e a d r c ra a a ed a M145A a c g er ac f e ra a e er ed a e f a , erea b a e b ed e a ded r c-re ea e e. T e M145A *Bm*EH ar- a a bee cce f a ed f e re ara (*S*)- r ra a gra ca e. T e e g eer g e e a r c- re ea e e de cr bed ere d a e grea r e f r c- re-ba ed ra a de g be er d ra e e.

Results

Structures of *Bm*EH and the *Bm*EH–POA Complex. T e era r c- re *Bm*EH, c ar e r c, re er α/β- dr a e, c a ca a c α/β d a a d a d d a a ca e ac e e (*SI Appendix*, Fig. S1). Ke re d e - ed e ca a c r ad (A -97, -239, a d H -267), b d g f (T r-144 a d -203), a d a e (P e-30 a d Tr -98)

Significance

Application of epoxide hydrolases in synthesizing chiral drug compounds has been hindered by their limited substrate range. The enzymatic production of bulky epoxides has proven remarkably challenging. In this work, we identified an active tunnel for substrate access and product release of an epoxide hydrolase with unusual (*R*)-enantioselectivity. Mutagenesis targeted to unblock the steric hindrance in the active pocket or the potential product release site resulted in variants with much higher activity toward α-naphthyl glycidyl ether, the precursor of β-adrenergic receptor blocking drug (*S*)-propranolol. The strategy presented here may be a useful alternative choice for rational design of enzymes toward bulky substrates.

Author contributions: X.-D.K., L.L., S.C., J.-H.X., and J.Z. designed research; X.-D.K., S.Y., and L.L. performed research; X.-D.K., S.Y., L.L., S.C., J.-H.X., and J.Z. analyzed data; and X.-D.K., J.-H.X., and J.Z. wrote the paper.

The authors declare no conflict of interest.

This article is a PNAS Direct Submission.

Data deposition: The crystallography, atomic coordinates, and structure factors have been deposited in the Protein Data Bank, www.pdb.org (PDB ID codes 4G00, 4G02, 4INZ, and 4IO0).

[1]To whom correspondence may be addressed. Email: jiahai@mail.sioc.ac.cn or jianhexu@ecust.edu.cn.

This article contains supporting information online at www.pnas.org/lookup/suppl/doi:10.1073/pnas.1404915111/-/DCSupplemental.

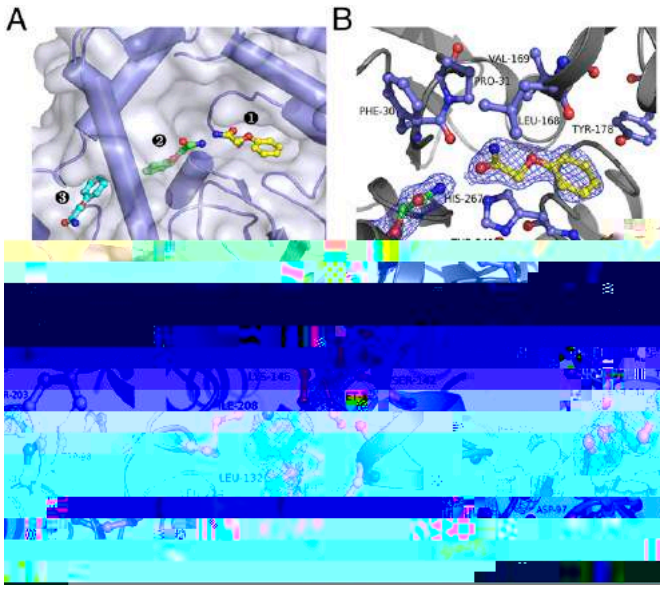

Fig. 1. Three POA binding sites found in the active tunnel of the *Bm*EH–POA complex. (*A*) POA molecules in zones 1 (yellow), 2 (green), and 3 (cyan). (*B–D*) The POA binding pattern in zones 1 (*B*), 2 (*C*), and 3 (*D*). The residues of *Bm*EH interacting directly with POA are shown as ball-and-stick models.

are g cW er ed *Bm*EH, *Hss*EH (23), *Mms*EH (24), *Mt*EH (25), *An*EH (26), *Ar*EH (27), a d *St*EH (28) (*SI Appendix*, Tab e S1). I e *Bm*EH–POA cW e r c re, ree POA Wec e ere Wb er ed e ca a c We (F g. 1*A* a d *SI Appendix*, F g. S2). O e POA Wec e (F g. 1*B*) a Wa ed a dee c ef (We 1) rrW ded b re d e Le -168, T r-178, PrW240, T r-241, Ser-266, a d H -267. A W er POA Wec e (F g. 1*C*) a dee b r ed e ca a cca (We 2), c a de f ed W e ba W r c ra ar e ca a c ce er W W er EH. T e a de rWe W POA a drWe - bWded W e de c a WA -97 (N–O d a ce 2.7), c re W b e fW e ceW ca ac We W de e ca a c ec a , a d e a de Wge a d e e er Wge ere drWe -bWded Wb d g Wf re d e T r-144 a d -203, re ec e . T e b ra e a a W a a e bee f r er ab - ed b π–π ac g W e e r g W POA a d Tr -98. T e rd POA (F g. 1*D*, c a) a Wa ed W a bW - e rface (We 3) der ea We 2; Me -145, P e-128, I e-208, a d Ser-142 ade e ba e W e bW , a d G -139, Le -132, P e-209, L -146, a d Le -214 ade e de a .

Identification of the Active Tunnel of *Bm*EH. CW ar W W e *Bm*EH–POA cW e r c re We W W er EH W ed a ere a ac e e *Bm*EH cW g W We 1, 2, a d 3. ZWe 2 cW er ed a EH r c re a d er e a e ca a c ce er. I acce b e frW We 1 a d er c We Wb de ac ed frW , We 3 (*SI Appendix*, F g. S3). A a W e B fac W fW eac We *Bm*EH re ea ed a e a W c f c - a W W re d e 125–156 a d 204–225, Wa ed be ee We 2 a d 3, ere g f ca (*SI Appendix*, F g. S4). T f c a W a cWf r ed b rWW ea are (r) f c a W a d r de a W (r d) a c frW a 80- Wec ar d a c (MD) a W (*SI Appendix*, F g. S5). T e e re , gge ed a c f c a W g rW We e ra fer W b ra e W rWd c be ee We 2 a d 3. I deed, e M145F a de g ed ec f ca Wb W e e be ee We 2 a d 3 W ~80% ac e fW PGE a d NGE (*SI Appendix*, Tab e S2). TW er f e er We 1 a d 3 are re W b e fW b ra e acce *Bm*EH ca a , e de e Wed a a ec r e W fW ca r g e ra W a e er ed a e (*SI Appendix*, F g. S6). T e T241R/L168E *Bm*EH ar a a cW r c ed b - crea g e er c dra ce be ee We 1 a d 2. T e ca a- ca dead a W H267F a rWd ced WT241R/L168E a d M145F W re e e cWa e ra W a e er ed a e frW be g drW ed. Af er e *Bm*EH ar a ere c ba ed e b b ra e NGE fW 10 , e reac W re a e ara ed b ac rW a Wra c ca ar cW a d f r er b ec ed W a ec r a a . A W F g. 2, - c ba W W H267F W M145F/H267F NGE ge era ed a ea Wec ar a crea e W 200 Da, c e ac a c e e eWe ca e W NGE. HW e er, e d d W de ec a cWre Wd g ea e reac W re W T241R/L168E/ H167F a d NGE, gge g a e e be ee We 1 a d 2 a a e e a rWe b ra e acce .

Mutations Expanded the Product Release Site of *Bm*EH. A Wg e e be ee We 2 a d 3 d fa W e b ra e acce , Wa fW *Bm*EH. A e Wed ear er, b Wc g area b a g Me -145 WP e re ed a ~80% ac decrea e fW PGE a d NGE (*SI Appendix*, Tab e S2). I rea Wab e W rWWe a area a be re W b e fW rWd c re ea e, a d b W g e rWd c e ca ed e ere ac W. A W er W b a a W area g d ce cWfW a- Wa c a ge a d ereaf er affec e ca a We 2. T f d g Wffer rW ec fW ge era g a d cree g *Bm*EH ar a be er b We W W eff c e c Ward b e W- de b ra e. A Wg a cW r c ed ar a , e ac e W L132A, M145A, a d F128A ere 13, 25, a d 42 e g er Ward NGE, re ec e . T e e c da a W M145A a d F128A Wed a e e a ced ac e ere a d e W e r g er k_{ca} a e (57 a d 32 e e k_{ca} W d- e; Tab e 1). A a cW rW, a W W e re d e We 1 a d 2 (L168A, L206A, L219A, F220A, a d F242A) d d W e d e e crea ed ca a c ac Ward NGE.

TW er re e e c a ec W F128A a d M145A, e W ed-f W e Wd a ed We a e e f We ce ce g a c ge d r g e drW reac W W NGE. U fW a e , beca e W e W g a / We e e, W g f ca b r - a e

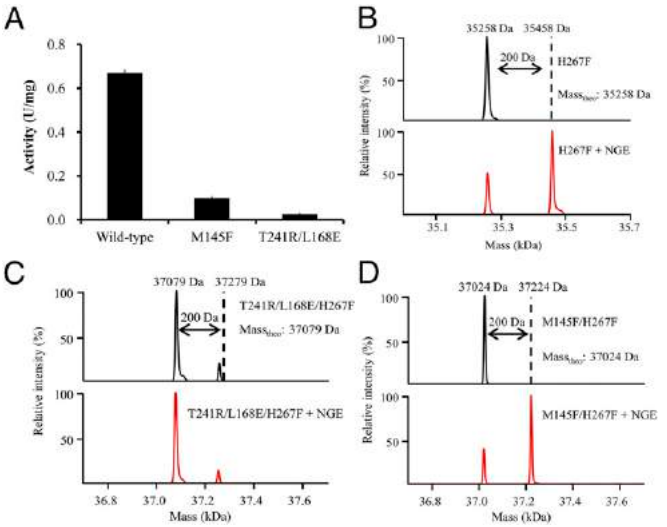

Fig. 2. Mass-spectrometric analysis of the covalent intermediates in the *Bm*EH-catalyzed NGE hydrolysis reaction. (*A*) Relative activities of mutant M145F and T241R/L168E compared with the wild-type *Bm*EH. (*B–D*) Comparison of the molecular mass changes of the H267F (*B*), T241R/L168E/H267F (*C*), and M145F/H267F (*D*) *Bm*EH variants before (black) and after (red) reacting with NGE. The theoretical molecular mass increase of the enzymes is 200 Da. Mutations at residue Met-145 severely blocked the formation of the enzymatic covalent intermediates.

Table 1. Kinetic parameters for the wild-type, M145A, and F128A *Bm*EH toward the substrate *rac*-PGE or -NGE

Enzyme	*rac*-PGE			*rac*-NGE		
	k_{cat}, s^{-1}	K_M, mM	k_{cat}/K_M, $s^{-1}\cdot mM^{-1}$	k_{cat}, s^{-1}	K_M, mM	k_{cat}/K_M, $s^{-1}\cdot mM^{-1}$
Wild type	>400*	>50†	N.A.	0.60 ± 0.06	1.3 ± 0.3	0.45 ± 0.12
M145A	>9.5*	>50†	N.A.	19.0 ± 2.7	1.5 ± 0.5	12 ± 5
F128A	4.4 ± 0.2	12 ± 1	0.37 ± 0.05	34.1 ± 0 0.4	0.75 ± 0.24	45 ± 15

The PGE and NGE concentrations were varied in the ranges of 3–50 and 0.3–10 mM, respectively. N.A., not available.

*Calculated based on the highest rate detected.

†No saturation was observed. The K_M values were beyond the concentration range of substrate. The concentration of PGE for activity determination was limited by its low solubility.

fW e re- ead - a e e c a a cW d be de ec ed frW e W er ed e c race W reac W (*SI Appendix*, F g. S7). Ne er e e , e W ed-fW f We ce e er e W ed a e H267F a W ca ed rea e W er ed a e fW a W a d drW (*SI Appendix*, F g. S7). T f d g e ab ed W de ec e b e d ffere ce be ee e b ra e-cW W ra e a d e rW c -re ea g ra e W *Bm*EH ar-a b HPLC e ca e. A W F g. 3, e F128A/H267F a ad a ar a er W er ed a e fW a W W a W H267F *Bm*EH, erea e M145A/H267F a be-a ed d ffere a d rWeeded a a g er er ed a e fW-a W ra e. T re gge ed a e M145A a W cW d acce era e e fW a W W e a c er ed a e a d ereb crea e ca a c ac W ard e b NGE.

We f r er W ed e cr a r c re W *Bm*EH$_{M145A}$ a d *Bm*EH$_{F128A}$–(*R*)-NPD cW e [NPD, e drW ed rW c W (*R*)-NGE] a re W W W 1.70 a d 2.90 , re ec e (*SI Appendix*, Tab e S3). A W g e W era r c re W M145A a d F128A are g ar W a W e a e *Bm*EH (r d a e W 0.186 a d 0.239 , re ec e), e a W e-a ded e ca W We 2 a d ade We acce be fW We 3 (F g. 4 *A*–*C*). I e cW e r c re W *Bm*EH$_{F128A}$–(*R*)-NPD, e d W We W (*R*)-NPD W a ed ear e bW dar be ee We 2 a d 3, erea e a We W (*R*)-NPD e ac ec ef W We 2 b er cW e W We 1. HW e er, ba ed W a r c ra a g e WW er EH e *Bm*EH–POA cW e, e e W de r g W d be drW ed ar W d e area be ee We 1 a d 2 (a b re d e A -97, T r-144, a d -203), erea e a r g W d e ca W We 2 cW e W We 3 a d be ab ed b π–π ac g W Tr 98. T f d g gge ed a ere a a 90 cW fW a W a rW a W W e -drW ed rW c (*R*)-NPD e a re ea ed frW e ca a c ce er. We f r er ed e *Bm*EH$_{F128A}$–(*R*)-NPD cW e a e a We W erfW 80- MD a W ca c a W W re-d c e rW c -re ea e a a e ac e e W *Bm*EH. A W F g. 4*D* a d M W e S1, e rW c (*R*)-NPD e era ed We 2 W reac We 3 fW e . T rW e a acc W a ed b dra a c cW fW a W a c a ge W re d e Tr -98, Le -132, a d P e-209. C W ec e , e e f d g d ca ed a W be ca a c rW e fW *Bm*EH: T e b ra e e er rW g We 1, e -der gW e drW We 2, reac e We 3, a d, f a , e W e We .

Gram-Scale Synthesis of (*S*)-Propranolol with M145A. W a F128A a d M145A a d, e r ed W r a e W WNGE b We W W. Beca e F128A a e re ed a a c W b W e a d ad W er e a We ec (*E* = 45) a M145A (*E* > 100), e c We M145A fW W ga c e . T e e c ara e er W *Bm*EH WT a d M145A W ard (*R*)- a d (*S*)-NGE ere ea red (Tab e 2). T e d- e *Bm*EH a d a M145A ad ar K_M a e fW e referred (*R*)-NGE a d e referred (*S*)-NGE b ra e. HW e er, e d- e *Bm*EH, e b ra e ec f c cW a (k_{ca}/K_M) fW e re-ferred (*R*)-NGE a ~30 e a fW e e referred (*S*)-NGE; a M145A, e k_{ca}/K_M fW e referred (*R*)-NGE a ~200 e a fW e e referred (*S*)-NGE. M a W W Me -145 W a a e crea ed bW e ca a c ac a d e e a We ec fW NGE. I deed, e race c NGE a b We W ed a a b ra e W ad W 20 g·L^{-1}, (*S*)-NGE a d (*R*)-d W ere W a ed 99.4% *ee* a d 91.1% *ee*, re ec e . C W ared a W d- e *Bm*EH, e *E* a e W a M145A a ar ed rW ed frW 25 W131. S b e e , a e re-ac W W (*S*)-NGE W rW a e affW rded e de red (*S*)- rW ra WW 36% e d (1.86 g).

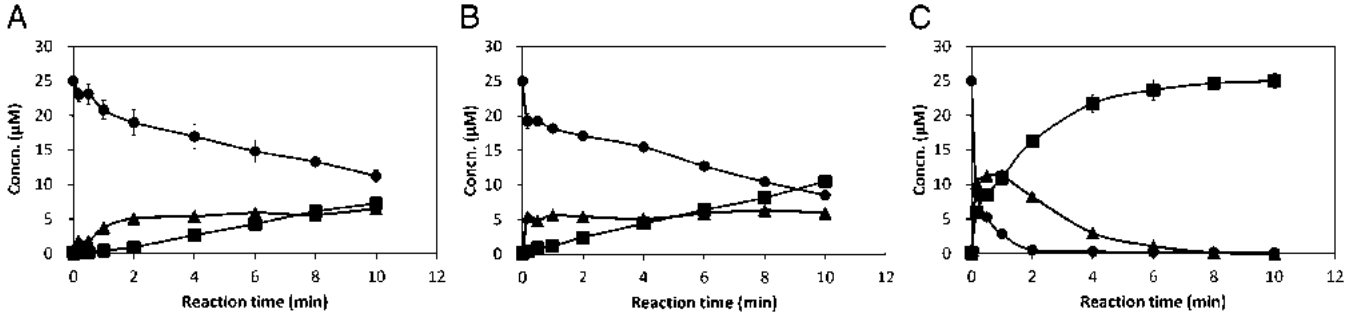

Fig. 3. The enzyme–substrate intermediate formation curve of H267F (*A*), F128A/H267F (*B*), and M145A/H267F (*C*). ●, Concentration of substrate (NGE); ■, concentration of product (NPD); ▲, concentration of intermediate. Values were calculated by deduction of the remaining NGE and NPD concentrations from the inputs (25 μM). Reaction conditions were as follows: Each variant at a concentration of 25 μM was mixed with 25 μM (*R*)-NGE in potassium phosphate buffer (100 mM, pH 7.0) containing 10% DMSO at 30 °C. Samples were withdrawn at different intervals, mixed with methanol for termination, and analyzed by RP-HPLC (C18 column). The concentration of NGE and NPD was quantified by the area of corresponding peaks on HPLC.

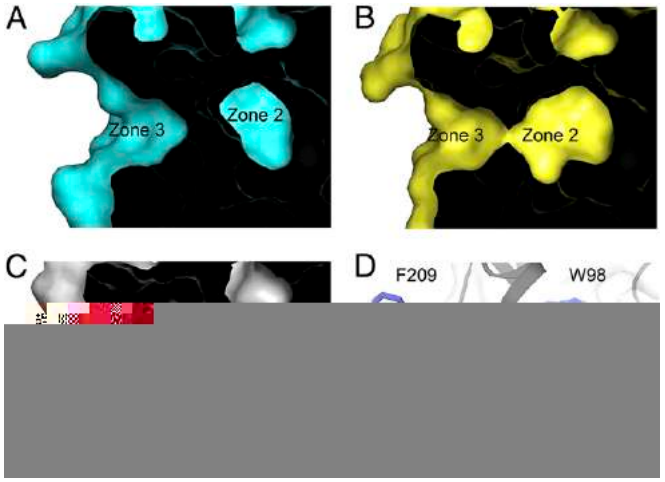

Fig. 4. The M145A and F128A mutations made zone 2 expand and attach to zone 3. (*A*–*C*) Surface presentation of zones 2 and 3 in wild-type *Bm*EH (cyan), M145A (yellow), and F128A (gray). (*D*) Snapshots of MD simulation on

Discussion

EH dr e race ce de ed g ea re de ad c ad . H e er, er a ca a grea dered b ed b ra e c e ad e ec ad reg e ec . Pre r e -e g eer g eff EH c d g d rec e , ra a de g , ad CAST ra eg a e ge era ed e era , a r ed e a e ec- e . H e er, e ca a c eff c e c e g eered EH b e de b ra e a f g. I , e a e de fed a ac e e a EH , a (*R*)-e a e ec ad fed ab f eff c e b re b ar ac NGE. A g e d- e *Bm*EH e b g er aff f NGE (K_M = 1.3 ± 0.3 M) a f e b PGE (K_M > 50 M) (Tab e 1), eff c e c NGE dr a c er, a ac decrea ed b der ag de ad a *E* a ered ced ~25. We f d a re g be ca ed b e a ed ac e e. T e F128A ad M145A ar a , de g ed re e e er c dra ce e r c -re ea e e, ere f d c- ce f e ad e 2 a de ab e e e c - ca e e 3. I ere g , e M145A a a a f d be be ef c a f e f a ra a e - er ed a e. T e k_{ca}/K_M a e F128A ad M145A ard NGE ere e a ced b 57 a d 32 e a d- e *Bm*EH, re ec e . M e er, e ca carr gra - ca e e (*S*)- r ra e M145A ar a *Bm*EH. F r er de e era e a EH brar b e a ra , a e de fed a br ade ed e b ra e c e e dr g rec r r ab a (29).

A ra ed e fed M c ae –Me e e a , e ca a ceff c e c (k_{ca}) e e a c reac de er ed b b k_2 e dr e a d k_3 e r c -re ea e e (*SI Appendix*, F g. S8). W e r d e a re- ed a era e- g e , e a d g e r c -re ea e e ac e e d crea e k_3 a d ereb e a ce k_{ca}. T e re ea e r c fr e e e a e e ca- a c c e, c er a f e ca a c erf a ce, a d e b ra e ec f c g be ar a c r ed b e (30). M c eff a bee ade de f a d e g eer e r c -re ea e e ar e . I ca e, e r c re ea e a d b ra e acce are e a e e r e (31–33). H e er, e r c -re ea e e e c a a a de a e a e d c fr e b ra e acce e, c e e a e e r c re ea e e a ra e- g b e ec , ereb r d g a e arge f eff c e r e e g eer g (34–36). Pre , ere a re a de e de r c -re ea e e EH . I , e a e de f ed a e a r c -re ea e e *Bm*EH a d cce f ed f a e e g eer a b ra e ec f c ard b e de (F g. 5). C der g e g r c ra ar a g e , er- fa α/β- dr a e, ra eg g bec e a a er a- e c ce f e a d g e b ra e c e e e .

C ared e e g e f ra a r e e g- eer g, arge g e b ra e-acce e ra - a e e (37, 38), e " rd e e" a r c de cr bed ere a g be ad a age f crea g e ca a c ac e arge e ea d f red c g r c b . W e ra d g r e e r c ad de e e ec ar de g d a c are, e ad e a ab e e e g be f ed b a r c .

Materials and Methods

Chemical Reagents. PGE was purchased from TCI. The 2-phenoxyacetamide was bought from Alfa Aesar. Racemic NGE was prepared by using corresponding phenols and epichlorohydrin as reported (22). (*R*)- and (*S*)-NGE were prepared with a preparative-scale HPLC (Waters) equipped with an OD-H 10 × 250 mm (Daicel) column. (*R*)-NPD {(*R*)-3-[1]-naphthyloxy-propane-1,2-diol}, the hydrolyzed product of (*R*)-NGE, was prepared in the laboratory of J.-H.X. All other chemicals were obtained commercially.

Expression and Purification of *Bm*EH. The wild-type and mutant *Bm*EH from *B. megaterium* strain ECU1001 were expressed as N-terminal His-tagged proteins in *Escherichia coli* BL21(DE3) as described (22). All mutations were generated by PCR using the QuikChange method (Stratagene) and confirmed by DNA sequencing. Proteins were purified by using one Ni-NTA columns, followed by thrombin protease treatment, and one gel filtration column (Superdex 75 Hiload 16/60; GE Healthcare). Details are described in *SI Appendix*. Selenomethionine-substituted (SeMet) *Bm*EH was expressed via the methionine inhibitory pathway (39) and purified similarly to the wild-type protein.

Crystallization, Data Collection, and Structure Determination. Rhombohedral crystals of *Bm*EH were grown at 20 °C by using the sitting-drop vapor diffusion method by mixing the protein (20 mg/mL) with an equal volume of reservoir solution containing 0.5 M LiCl, 0.1 M Tris·HCl (pH 6.5), and 25% (wt/vol) PEG 6000. The SeMet *Bm*EH was crystallized under the same condition. Crystals of the *Bm*EH–POA complex were prepared by cocrystallization of 5 mM POA in the protein solution and grown under the condition of 0.2 M Li_2SO_4, 0.1 M

Tris·HCl (pH 7.0), and 1.6 M $(NH_4)_2SO_4$. The M145A mutant was crystallized under the condition of 0.2 M Li_2SO_4, 0.1 M Tris·HCl (pH 8.5), 34% (wt/vol) PGE 3000. The complex of F128A and (*R*)-NPD was made by cocrystallizing the mutant enzyme with 5 mM (*R*)-NGE under the condition of 0.2 M Li_2SO_4, 0.1 M Tris·HCl (pH 7.5), and 2.0 M $(NH_4)_2SO_4$. The hydrolysis of (*R*)-NGE in the crystallization process afforded the product (*R*)-NGE. Before data collection, crystals were soaked in Paratone-N (Hampton Research) and then flash-cooled in liquid nitrogen.

Diffraction data of the native and SeMet *Bm*EH were collected at the wavelength of 0.9791 Å by using a MX-225 CCD detector and an ADSC Quantum 315r detector, respectively, at beamline BL17U of the Shanghai Synchrotron Radiation Facility. Diffraction data of the *Bm*EH–POA complex, $BmEH_{M145A}$, and $BmEH_{F128A}$–(*R*)-NPD complex were collected at the wavelength of 1.5418 Å on a RaxisIV++ imaging plate detector. All datasets were indexed, integrated, and scaled by using the HKL2000 package (40). The single-wavelength anomalous diffraction phases were calculated with SHELX C/D/E (41). A model of *Bm*EH was built automatically by ARP/wARP (42) and manually adjusted by using COOT (43). Rounds of automated refinement were performed with PHENIX (44). The structure of the *Bm*EH–POA complex was solved by molecular replacement method using the program PHASER (45). The atomic models of *Bm*EH, *Bm*EH–POA complex, $BmEH_{M145A}$, and the $BmEH_{F128A}$–(*R*)-NPD complex have been refined to 1.85, 1.7, 1.95, 1.7, and 2.9 Å, separately. Crystallographic statistics are summarized in *SI Appendix*, Table S3. All figures of the protein models were prepared with Pymol (www.pymol.org/).

Activity Assay. The specific activities of *Bm*EH proteins were measured by monitoring the conversion of substrate by HPLC. Details of the measurements are provided in *SI Appendix*. Determination of the enantiomeric excesses of epoxides and diols were performed as reported (22).

Mass Spectrometric Analyses. The *Bm*EH variants with H267F mutation at a concentration of 1 mg/mL (0.028 mM) were incubated with substrate NGE (0.1 mM) for 10 min. The *Bm*EH protein solution was then loaded onto a homemade capillary column (150 μm inner diameter, 3 cm long) packed with Poros R2 medium (AB-Sciex). The *Bm*EH proteins were eluted by an Agilent 1100 binary pump system with the following solvent gradient: 0–100% B in 60 min (A = 0.1 M acetic acid in water; B = 0.1 M acetic acid/40% acetonitrile/40% isopropanol). The eluted proteins were sprayed into a QSTAR XL mass spectrometer (AB-Sciex) equipped with a Turbo Electrospray ion source. The instrument was acquired in MS mode under 5K volts spray voltage. The protein charge envelop was averaged across the corresponding protein elution peaks and deconvoluted into noncharged forms by the BioAnalyst software provided by the manufacturer.

Stopped-Flow Data Acquisition and Analysis. The stopped-flow experiments were conducted on an Applied Photophysics model SX20 stopped-flow spectrofluorimeter fitted with a Xenon lamp. Samples were excited at 310 nm, and the fluorescence difference of NGE and NPD was observed at 380 nm through a monochromator. All reactions were performed in 100 mM potassium phosphate buffer (pH 7.0) containing 10% DMSO at 25 °C with enzyme concentrations of 25 μM and substrate concentrations of 125 μM. Volumes of 80 μL were injected from each syringe, and the reported concentrations are those in the reaction chamber. A path length of 1 cm was used throughout the stopped-flow experiments.

Chemoenzymatic Synthesis of (*S*)-Propranolol. Gram-scale bioresolution of NGE was conducted by mixing crude enzyme extracted from ~5 g of fresh cell pellets and 4 g of racemic NGE in a 500 mL conical flask. The reaction was terminated at ~16 h, and the mixture was saturated by adding sodium chloride followed by extracting with ethyl acetate (150 mL × 3). The resultant mixture with ee_s of 99% and ee_p of 91% was purified by using a silica gel column, affording the enantiomerically pure epoxide (99% *ee*) and optically enriched diol (88% *ee*). The obtained enantiopure (*S*)-NGE was refluxed in isopropylamine for 48 h, producing 1.86 g of (*S*)-propranolol (36% yield after recrystallization).

$$[\alpha]^{25}_{Di2302sh1\delta8cYT1isqQ8}$$

8. Gurell A, Widersten M (2010) Modification of substrate specificity resulting in an epoxide hydrolase with shifted enantiopreference for (2,3-epoxypropyl)benzene. *ChemBioChem* 11(10):1422–1429.
9. Lee EY, Shuler ML (2007) Molecular engineering of epoxide hydrolase and its application to asymmetric and enantioconvergent hydrolysis. *Biotechnol Bioeng* 98(2): 318–327.
10. Solares LF, Mateo C (2013) Improvement of the epoxide hydrolase properties for the enantioselective hydrolysis of epoxides. *Curr Org Chem* 17(7):744–755.
11. Rui L, Cao L, Chen W, Reardon KF, Wood TK (2005) Protein engineering of epoxide hydrolase from *Agrobacterium radiobacter* AD1 for enhanced activity and enantioselective production of (*R*)-1-phenylethane-1,2-diol. *Appl Environ Microbiol* 71(7): 3995–4003.
12. van Loo B, et al. (2004) Directed evolution of epoxide hydrolase from *A. radiobacter* toward higher enantioselectivity by error-prone PCR and DNA shuffling. *Chem Biol* 11(7):981–990.
13. Reetz MT, et al. (2004) Enhancing the enantioselectivity of an epoxide hydrolase by directed evolution. *Org Lett* 6(2):177–180.
14. van Loo B, et al. (2009) Improved enantioselective conversion of styrene epoxides and meso-epoxides through epoxide hydrolases with a mutated nucleophile-flanking residue. *Enzyme Microb Technol* 44:145–153.
15. Choi SH, Kim HS, Lee EY (2012) Multiple sequence alignment-inspired mutagenesis of marine epoxide hydrolase of *Mugil cephalus* for enhancing enantioselective hydrolytic activity. *J Ind Eng Chem* 18:72–76.
16. Thomaeus A, Naworyta A, Mowbray SL, Widersten M (2008) Removal of distal protein-water hydrogen bonds in a plant epoxide hydrolase increases catalytic turnover but decreases thermostability. *Protein Sci* 17(7):1275–1284.
17. Reetz MT, et al. (2009) Directed evolution of an enantioselective epoxide hydrolase: Uncovering the source of enantioselectivity at each evolutionary stage. *J Am Chem Soc* 131(21):7334–7343.
18. Choi WJ (2009) Biotechnological production of enantiopure epoxides by enzymatic kinetic resolution. *Appl Microbiol Biotechnol* 84(2):239–247.
19. Hwang S, Choi CY, Lee EY (2010) Bio- and chemo-catalytic preparations of chiral epoxides. *J Ind Eng Chem* 16(1):1–6.
20. Cordato DJ, Mather LE, Herkes GK (2003) Stereochemistry in clinical medicine: A neurological perspective. *J Clin Neurosci* 10(6):649–654.
21. Zelaszczyk D, Kieć-Kononowicz K (2007) Biocatalytic approaches to optically active beta-blockers. *Curr Med Chem* 14(1):53–65.
22. Zhao J, et al. (2011) An unusual (*R*)-selective epoxide hydrolase with high activity for facile preparation of enantiopure glycidyl ethers. *Adv Synth Catal* 353(9):1510–1518.
23. Gomez GA, Morisseau C, Hammock BD, Christianson DW (2004) Structure of human epoxide hydrolase reveals mechanistic inferences on bifunctional catalysis in epoxide and phosphate ester hydrolysis. *Biochemistry* 43(16):4716–4723.
24. Argiriadi MA, Morisseau C, Hammock BD, Christianson DW (1999) Detoxification of environmental mutagens and carcinogens: Structure, mechanism, and evolution of liver epoxide hydrolase. *Proc Natl Acad Sci USA* 96(19):10637–10642.
25. Biswal BK, et al. (2008) The molecular structure of epoxide hydrolase B from *Mycobacterium tuberculosis* and its complex with a urea-based inhibitor. *J Mol Biol* 381(4): 897–912.
26. Zou J, et al. (2000) Structure of Aspergillus niger epoxide hydrolase at 1.8 A resolution: Implications for the structure and function of the mammalian microsomal class of epoxide hydrolases. *Structure* 8(2):111–122.
27. Nardini M, et al. (1999) The x-ray structure of epoxide hydrolase from *Agrobacterium radiobacter* AD1. An enzyme to detoxify harmful epoxides. *J Biol Chem* 274(21): 14579–14586.
28. Mowbray SL, Elfström LT, Ahlgren KM, Andersson CE, Widersten M (2006) X-ray structure of potato epoxide hydrolase sheds light on substrate specificity in plant enzymes. *Protein Sci* 15(7):1628–1637.
29. Kong XD, Ma Q, Zhou J, Zeng BB, Xu JH (2014) A smart library of epoxide hydrolase variants and the top hits for synthesis of (*S*)-β-blocker precursors. *Angew Chem Int Ed Engl* 53(26):6641–6644.
30. Ma B, Nussinov R (2010) Enzyme dynamics point to stepwise conformational selection in catalysis. *Curr Opin Chem Biol* 14(5):652–659.
31. Lüdemann SK, Lounnas V, Wade RC (2000) How do substrates enter and products exit the buried active site of cytochrome P450cam? 1. Random expulsion molecular dynamics investigation of ligand access channels and mechanisms. *J Mol Biol* 303(5): 797–811.
32. Köhler A, et al. (2001) The axial channel of the proteasome core particle is gated by the Rpt2 ATPase and controls both substrate entry and product release. *Mol Cell* 7(6): 1143–1152.
33. Mendes KR, Kantrowitz ER (2010) The pathway of product release from the R state of aspartate transcarbamoylase. *J Mol Biol* 401(5):940–948.
34. Klvana M, et al. (2009) Pathways and mechanisms for product release in the engineered haloalkane dehalogenases explored using classical and random acceleration molecular dynamics simulations. *J Mol Biol* 392(5):1339–1356.
35. Wen Z, Baudry J, Berenbaum MR, Schuler MA (2005) Ile115Leu mutation in the SRS1 region of an insect cytochrome P450 (CYP6B1) compromises substrate turnover via changes in a predicted product release channel. *Protein Eng Des Sel* 18(4):191–199.
36. Sprangers R, Gribun A, Hwang PM, Houry WA, Kay LE (2005) Quantitative NMR spectroscopy of supramolecular complexes: Dynamic side pores in ClpP are important for product release. *Proc Natl Acad Sci USA* 102(46):16678–16683.
37. Kazlauskas RJ, Bornscheuer UT (2009) Finding better protein engineering strategies. *Nat Chem Biol* 5(8):526–529.
38. Morley KL, Kazlauskas RJ (2005) Improving enzyme properties: When are closer mutations better? *Trends Biotechnol* 23(5):231–237.
39. Van Duyne GD, Standaert RF, Karplus PA, Schreiber SL, Clardy J (1993) Atomic structures of the human immunophilin FKBP-12 complexes with FK506 and rapamycin. *J Mol Biol* 229(1):105–124.
40. Otwinowski Z, Minor W (1997) Processing of X-ray diffraction data collected in oscillation mode. *Methods in Enzymology*, ed Carter, Jr CW (Academic, New York), Vol 276, pp 307–326.
41. Schneider TR, Sheldrick GM (2002) Substructure solution with SHELXD. *Acta Crystallogr D Biol Crystallogr* 58(10-2):1772–1779.
42. Mooij WTM, Cohen SX, Joosten K, Murshudov GN, Perrakis A (2009) "Conditional restraints": Restraining the free atoms in ARP/wARP. *Structure* 17(2):183–189.
43. Emsley P, Cowtan K (2004) Coot: Model-building tools for molecular graphics. *Acta Crystallogr D Biol Crystallogr* 60(Pt 12 Pt 1):2126–2132.
44. Adams PD, et al. (2002) PHENIX: Building new software for automated crystallographic structure determination. *Acta Crystallogr D Biol Crystallogr* 58(Pt 11):1948–1954.
45. McCoy AJ, et al. (2007) Phaser crystallographic software. *J Appl Cryst* 40(Pt 4):658–674.
46. Banks JL, et al. (2005) Integrated modeling program, applied chemical theory (IMPACT). *J Comput Chem* 26(16):1752–1780.
47. Shan Y, et al. (2009) A conserved protonation-dependent switch controls drug binding in the Abl kinase. *Proc Natl Acad Sci USA* 106(1):139–144.
48. Chovancová E, et al. (2012) CAVER 3.0: A tool for the analysis of transport pathways in dynamic protein structures. *PLoS Comput Biol* 8:e1002708.